Variability in sinking fluxes and composition of particle-bound phosphorus in the Xisha area of the northern South China Sea

Yuan Dong[a], Qian P. Li[a,*], Zhengchao Wu[a], Jia-Zhong Zhang[b]

[a] State Key Laboratory of Tropical Oceanography, South China Sea Institute of Oceanology, Chinese Academy of Sciences, Guangzhou 510301, China
[b] Ocean Chemistry and Ecosystems Division, Atlantic Oceanographic and Meteorological Laboratory, National Oceanic and Atmospheric Administration, Miami, FL 33149, USA

ARTICLE INFO

ABSTRACT

Export fluxes of phosphorus (P) by sinking particles are important in studying ocean biogeochemical dynamics, whereas their composition and temporal variability are still inadequately understood in the global oceans, including the northern South China Sea (NSCS). A time-series study of particle fluxes was conducted at a mooring station adjacent to the Xisha Trough in the NSCS from September 2012 to September 2014, with sinking particles collected every two weeks by two sediment traps deployed at 500 m and 1500 m depths. Five operationally defined particulate P classes of sinking particles including loosely-bound P, Fe-bound P, $CaCO_3$-bound P, detrital apatite P, and refractory organic P were quantified by a sequential extraction method (SEDEX). Our results revealed substantial variability in sinking particulate P composition at the Xisha over two years of samplings. Particulate inorganic P was largely contributed from Fe-bound P in the upper trap, but detrital P in the lower trap. Particulate organic P, including exchangeable organic P, $CaCO_3$-bound organic P, and refractory organic P, contributed up to 50–55% of total sinking particulate P. Increase of $CaCO_3$-bound P in the upper trap during 2014 could be related to a strong El Niño event with enhanced $CaCO_3$ deposition. We also found sediment resuspension responsible for the unusual high particles fluxes at the lower trap based on analyses of a two-component mixing model. There was on average a total mass flux of 78 ± 50 mg m^{-2} d^{-1} at the upper trap during the study period. A significant correlation between integrated primary productivity in the region and particle fluxes at 500 m of the station suggested the important role of biological production in controlling the concentration, composition, and export fluxes of sinking particulate P in the NSCS.

1. Introduction

Phosphorus (P), an essential element for phytoplankton growth, plays an important role in marine ecosystem dynamics and eventually controls the productivity of the ocean over geological time scales (Tyrrell, 1999). Being a particle active species in seawater, dissolved inorganic phosphorus (DIP) is readily scavenged out of seawater by settling particles in the coastal environments (Ruttenberg and Berner, 1993). In the open ocean, DIP is incorporated into organic matter by phytoplankton and the fixed organic phosphorus is subsequently exported out of the euphotic zone by particles sinking to the deep ocean (Benitez-Nelson et al., 2007). As concentration of DIP is often very low in the surface ocean, remineralization of sinking particulate organic phosphorus (POP) and subsequent upwelling of the regenerated phosphate in the thermocline are thus important mechanisms for sustaining phytoplankton production and the associated biological carbon pump (Bjorkman and Karl, 2003; Honjo et al., 2008).

Particulate phosphorus can be partitioned into organic and inorganic forms in the ocean due to their different consumption pathways. In the North Pacific Ocean, a large fraction of the settling particulate P was actually found in the sinking biogenic organic matter (e.g., Yoshimura et al., 2007), which is in contrast to the coastal waters where particulate inorganic phosphorus (PIP) often dominated sinking P fluxes (Faul et al., 2005; Lyons et al., 2011). The predominance of compounds derived from phytoplankton and zooplankton affects phosphorus composition of sinking particles, as the amount of sinking particulate materials below the euphotic zone would be constrained by primary productivity above (Benitez-Nelson and Buesseler, 1999; Francois et al., 2001). Variations in the inorganic-to-organic ratios of sinking particulate P should reflect the change of water column biogeochemistry (Sekula-Wood et al., 2012). It is therefore crucial to identify and quantify the various forms of inorganic and organic P in sinking particles and their associated export fluxes in order to fully understand the dynamic of P cycle in the ocean.
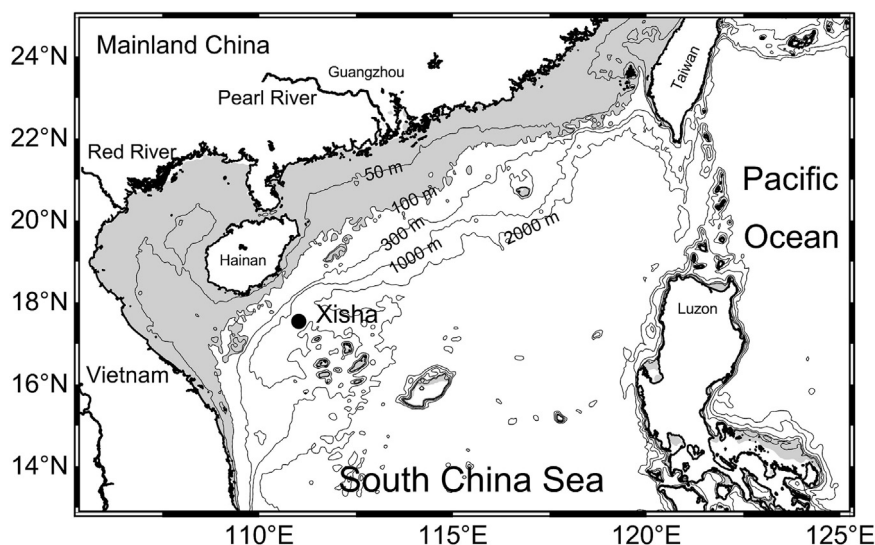
Fig. 1. Topography of the northern South China Sea (NSCS). Black dot is the Xisha (XS) station where mooring sediment traps were deployed with thin lines showing the bathymetry and the shaded area representing the NSCS continental shelf.

The northern South China Sea (NSCS) (Fig. 1), one of the world's largest semi-enclosed seas, is influenced by seasonal monsoons, upwelling/mixing, river discharges, internal waves, and eddies (Liu et al., 2002). Although DIP in the surface NSCS was very low, phytoplankton community was generally limited by nitrogen due to low nitrogen-to-phosphorus ratios of the surface seawater (Wu et al., 2003). P-limitation of primary production was found in the summer when the outflows of P-deficit riverine waters mixed with the oligotrophic NSCS waters (Yin et al., 2004; Xu et al., 2008). Export fluxes of particulate organic materials including POP at the base of the euphotic zone of the NSCS were higher in the winter-spring but lower in the summer-fall (Chen et al., 2008), due to seasonal variability of productivity (Wei et al., 2011). Vertical distributions of sinking particulate P in the NSCS were influenced by both primary production and P adsorption on mineral clays (Ho et al., 2009). One previous study has shown that POP was ~57% of the total particulate phosphorus (TPP) at 1000 m of the NSCS but detailed P speciation was lacking, not to mention the temporal variations of different P forms and their associated fluxes (Liebezeit, 1991).

In this paper, we report a time-series study of particle fluxes by sediment trap measurements from September 2012 to September 2014 at a mooring station of Xisha (named XS hereafter) in the western NSCS. The Xisha area was characterized by higher particulate organic carbon fluxes compared to the central NSCS (Ma et al., 2011). There was on average 65% of sinking particles at Xisha originating from Taiwan by advective transport and deposition, with relatively less contribution by the nearby Red River (Liu et al., 2014). Using a sequential extraction method (SEDEX) (Ruttenberg, 1992; Zhang et al., 2010), we quantified five classes of sinking particulate P from sediment trap samples, including loosely-bound P, Fe-bound P, $CaCO_3$-bound P, detrital apatite P, and refractory organic P. Based on these data, we examined the temporal variability of the particulate P concentration and composition, as well as the associated export P fluxes at XS. Our goals are to address the mechanisms responsible for long-term change of sinking particulate P and to understand the role of sinking particles on biogeochemical cycling of P in this high-productive marginal sea.

2. Material and methods

2.1. Descriptions of the study site, sediment trap moorings, and seawater samplings

The time-series mooring station (XS) is located at 17° 24.5′ N, 110°

55.0′ E with a bottom depth of 1690 m (Fig. 1). During the winter monsoon, a deepening mixed layer of ~60 m is typically found at XS (Fig. 2A). Nutrient profiles at XS are similar to the oligotrophic central NSCS (Li et al., 2015), with phosphate of < 0.1 μm, nitrate plus nitrite of < 1 μm and silicate of < 1.5 μm at the surface (Fig. 2B). Water column at XS is generally stratified in the summer with reduced nutrient supply leading to low productivity. Discrete samples were collected by SeaBird SBE 9/11 CTD aboard R/V *Shiyan III* during November 2013 with nutrients measured at lab by a Seal AA3 autoanalyzer (Bran-Luebbe, GmbH) and the surface low-level phosphate by a highly sensitive long-path spectrophotometry method (Li et al., 2008; Li and Hansell, 2008).

Two sediment traps (Nichiyu Giken Kogyo, SMD-26S) were deployed at the XS station from September 2012 to September 2014 at the depths of 500 m and 1500 m, respectively. Sample collection was made twice a month and each sample measures a 14–16 days accumulative flux (lower trap sampling was not performed after January 2014). The sediment trap had a collecting area of 0.5 m² and sampling cups were filled with particle free seawater (0.45 μm filtration) containing 3.3 g/L $HgCl_2$ to prevent microbial decomposition of organic matter. Particle samples were stored in polyethylene bottles at 4°C until further analyses. Larger zooplankton (such as foraminifers) was removed once the trap samples returned to the lab. The sample was then ground to < 125 μm and oven dried for 24 h before final dry-weight determination. Total mass flux (TMF in unit of mg m⁻² d⁻¹) of the sinking particles was obtained when the dry-weight was divided by the collecting area and the exposure time. Flux of each particulate P composition was estimated by multiplying P mass concentration with TMF.

2.2. Procedure of sequential extraction of particulate P from sediment trap samples

We used a modified five-step sequential extraction method (SEDEX) by Zhang et al. (2010) to separate various forms of P in the sediment trap samples: (1) loosely-bound P including adsorbed inorganic P and exchangeable organic P, (2) Fe-bound inorganic P, (3) $CaCO_3$-bound P that is the calcium-phosphate minerals of the apatite group including authigenic carbonate fluorapatite, biogenic apatite, $CaCO_3$ associated apatite, (4) detrital apatite P, and (5) refractory organic P (Ruttenberg, 1992). Soluble reactive phosphorus (SRP) and total dissolved phosphorus (TDP) of the extracted supernatant during each step were measured by methods in Section 2.3.
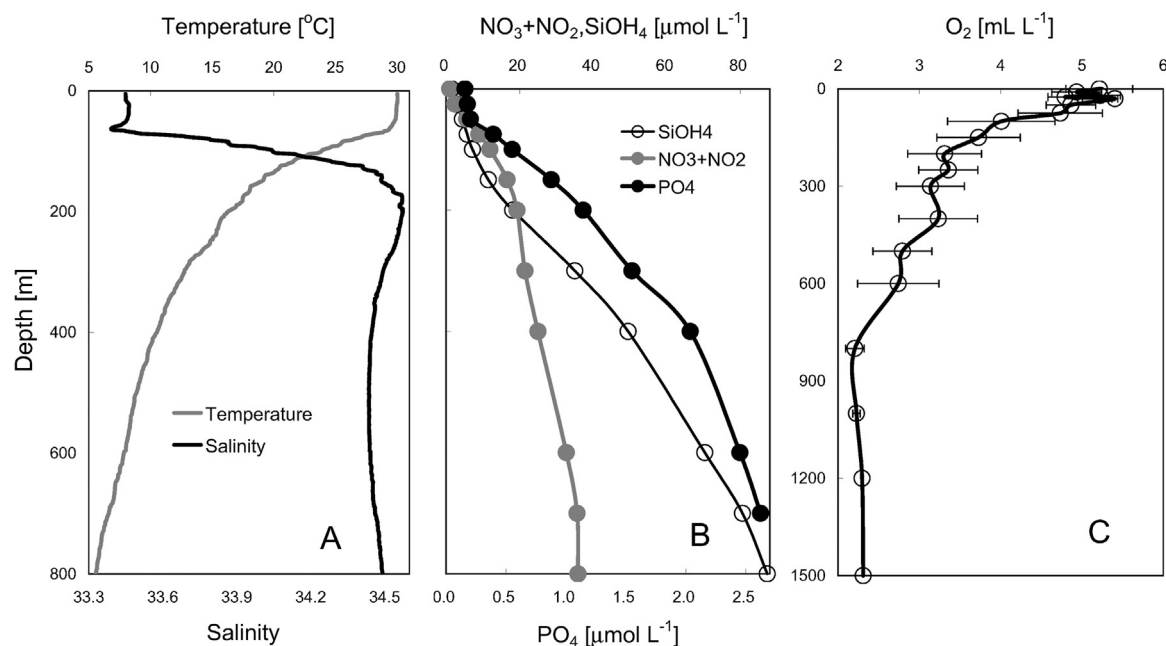
Fig. 2. Typical profiles of (A) temperature, salinity, (B) phosphate, silicate, and nitrate plus nitrite, and (C) dissolved oxygen at the XS station. Data of November 2013 are shown in (A) and (B); (C) are the average of 5 stations near the XS from the Word Ocean Database 2009.

Firstly, a dry sediment trap sample (0.5g) was added to a 40 ml 1 M $MgCl_2$ solution (pH=8.0) in a 50 ml polypropylene tube. After shaking for 2 h, the sample slurry was centrifuged. SRP and TDP were measured in the supernatant, thus the loosely adsorbed inorganic P was measure as the SRP and the exchangeable organic P can be calculated as a difference between TDP and SRP. Secondly, the residue from previous step was extracted by a 40 ml bicarbonate dithionite mixed solution (0.11 M $NaHCO_3$ and 0.11 M $Na_2S_2O_4$, pH =7.0) without citrate for 4 h. Supernatant after centrifuge was placed in a fuming hood for 72 h. Fe-bound P was estimated from the SRP of the supernatant. TDP measurement at this step was not made because it has been shown to be negligible in a previous study (Zhang et al., 2004) but it would be a good addition to verify the extent of OP associated with Fe in the XS samples. Thirdly, the residue was further extracted by a 40 ml acetate buffer solution for 6 h. The supernatant and the washing solution (precipitate was rinsed by 1 M $MgCl_2$) were determined for the SRP and the TDP. $CaCO_3$-bound inorganic P was measured by the SRP of the extraction with $CaCO_3$-bound organic P calculated as the difference between TDP and SRP. Fourthly, the residue from previous step was extracted by a 40 ml 1 M HCl solution for 16 h. Detrital apatite P was referred as the SRP of the supernatant after centrifuge. Finally, the remained solid sample was combusted at 550 °C for 2 h. At room temperature, the ashed sample was extracted by a 40 ml of 1 M HCl solution for 24 h. Refractory organic P was measured as the SRP of the final solution.

Total particulate phosphorus (TPP) in the sediment trap sample was estimated by adding up all the five P classes. However, if possible, a separate TPP measurement is also needed to estimate the recovery of SEDEX method. PIP was calculated by the sum of adsorbed inorganic P, Fe-bound P, $CaCO_3$-bound inorganic P, and detrital apatite P, whereas POP included exchange organic P, $CaCO_3$-bound organic P, and refractory organic P (Ruttenberg, 1992). The detection limit of SEDEX method is 0.01 µm depended on the accuracy of SRP measurement (Zhang et al., 2010).

2.3. Determination of SRP and TDP in the extracted solutions

SRP of the extracted solution was determined by phosphomolybdenum blue method using a UV–visible spectrophotometer with a detection limit of 0.01 µm and a precision of ~2% (Zhang et al., 2010). Phosphate standards were prepared by reagent-grade oven-dried KH_2PO_4 and all other chemicals, including ammonium molybdate, potassium antimony tartrate, and ascorbic acid, were of analytical grade. We followed the reagent recipe of Zhang et al. (2010) to accommodate the acidity of a given extraction for optimal color development during the experiments. Sample neutralization was performed only when pH of the extracted solution was beyond the buffering capability of the reagents.

We used a persulfate digestion method without pH adjustment (Huang and Zhang, 2009) to determine the TDP in the extraction. In short, a 2 ml of $K_2S_2O_8$ (20 g $K_2S_2O_8$ in 400 ml Milli-Q water, pH=6.5) solution was mixed with a 10 ml of the extracted solution in a Teflon vial, which was then firmly capped and placed in an oven. Digestion was processed in the oven at 90°C for 16 h. A 3 ml of phosphate reagent was added to the digested solution when the vial cooled down to a room temperature. After 8 min of color development under the room temperature, TDP of the extraction was quantified by measuring the SRP of the final solution. Dissolved organic P of the extracted solution was then calculated by the difference between TDP and SRP.

2.4. Determination of biogenic silica in sinking particles

Biogenic silica of sinking particles was extracted by a Na_2CO_3 solution (Mortlock and Froelich, 1989). Specifically, a 5 ml of 10% H_2O_2 was added to a 150 mg of dried particle sample in a 50 ml polypropylene tube containing and exposed them to the air for 30 min. After adding a 5 ml of 1N HCl, the tube was tightly capped and sonicated for 30 min. These steps removed the adsorbed carbonate and organics on the particle surface. After adding a 20 ml of Milli-Q water, the sample was centrifuged at 6000 rpm for 5 min. The solid remainder was collected by filtration and supernatant was discarded. A 40 ml of 2 M Na_2CO_3 solution was added to the solid sample in a sample tube then placed them in a water bath at 85 °C for 5 h. A pin-hole was made for each tube cap in this step to allow gas expansion during the heating, with water replenished every two hours to compensate evaporation in the water bath. After the hot bath, the tubes were centrifuged at 6000 rpm for 5 min. Supernatants were collected and measured by a standard colorimetric method (Mortlock and Froelich, 1989).

Specifically, an aliquot of 1.25 ml of supernatant from centrifuge was determined for dissolved silicate immediately by molybdate-blue method at room temperature using a UV–Visible spectrophotometer at a wavelength of 812 nm.

2.5. Remote sensing observations

The depth-integrated primary productivity (IPP), acquired from the US National Climatic Data Center, was derived from several satellite measurements including chlorophyll-*a* concentration and photosynthetically available radiation from the Aqua MODIS sensor aboard the GeoEye spacecraft and sea surface temperature from the NOAA's Pathfinder Project based on algorithm of the Vertical Generalized Production Model (Behrenfeld and Falkowski, 1997). Precipitation rate at XS was acquired from the NCAR's monthly Global Precipitation Climatology Project (GPCP). Multivariate El Niño/Southern Oscillation index (MEI) during our study period was acquired from NOAA's Earth System Research Laboratory.

3. Results and discussion

3.1. Five different classes of phosphorus-containing particles

The loosely-bound P of sinking particles, including adsorbed inorganic P and exchangeable organic P, can be readily released into water column by desorption processes and is one of the most important P sources for phytoplankton growth. The inorganic and organic fractions of loosely bound P at 500 m of the XS station were 6.4 ± 1.6 and 8.9 ± 2.6 µmol P g^{-1} in the summer, which were significantly higher ($t > 5.65$, $p < 0.01$, df=11) than those in the winter (2.7 ± 1.5 and 3.5 ± 0.9 µmol P g^{-1}) (Fig. 3A and B). In contrast, there was no clear seasonality for both of them at 1500 m (Fig. 3C and D). The fraction of loosely-bound P in TPP was on average $23 \pm 8\%$ in the upper traps and $11 \pm 6\%$ in the lower traps during our studies. These percentages were higher than those of the surface sediment particles (8%, e.g., Zhang et al., 2004) but lower than many suspended particles measured near coasts (Berner and Rao et al., 1994; Sutula et al., 2004; Lin et al., 2012).

Fe-bound P, the fraction of particulate P associated with iron oxide, has high chemical activity and can be closely related to the saturation level of dissolved oxygen at depth (Lyons et al., 2011). Fe-bound P at 500 m of XS varied substantially from 0.56 to 32.2 µmol P g^{-1} (Fig. 3B), whereas it was relatively constant (< 3 µmol P g^{-1}) at 1500 m (Fig. 3D). In the upper trap, Fe-bound P is much higher ($t=4.88$, $p < 0.01$, df=11) in the summer (17.9 ± 6.8 µmol P g^{-1}) than in the winter (7.7 ± 3.0 µmol P g^{-1}). On average, the contribution of Fe-bound P to TPP was $25 \pm 9\%$ at 500 m but $7 \pm 6\%$ at 1500 m. The upper trap samples have a percentage of Fe-bound P similar to Florida Bay surface sediment (Zhang et al., 2004). The lower content and percentage of Fe-bound P found in the lower trap near the seafloor may be due to low oxygen of the deep water (Fig. 2C), given that it would be readily converted to the SRP when the oxides undergo reductive dissolution in the low oxygenated waters (Lyons et al., 2011).

Due to strong P adsorption by carbonate minerals (Millero et al., 2001), conversions of organic, adsorbed, and Fe-bound P to CaCO$_3$ associated P were commonly found during particle sinking (Diaz et al., 2008). On average, the CaCO$_3$-bound P accounted for a $22 \pm 10\%$ of the TPP at XS, which were consistent with many of the sinking particles found in the west coast of USA (Faul et al., 2005; Lyons et al., 2011; Sekula-Wood et al., 2012). Although the total CaCO$_3$-bound P, including both its inorganic and organic fractions, was relatively constant at 1500 m (5.9 ± 3.6 µmol P g^{-1}) (Fig. 3C and D), there was a general increasing trend ($p < 0.01$) of the total CaCO$_3$-bound P with time at 500 m of the XS station, particularly during the year 2014 (Fig. 3A and B).

Detrital apatite P, the most inert part of PIP for biological remineralization, is mostly terrestrial origin and thus is not directly involved in marine P cycle. Although the absolute concentrations of detrital P in the sinking particles were similar between two depths (Fig. 3B and D), the percentage of detrital P to TPP at 500 m was significantly lower than at 1500 m. In the upper trap, detrital P was the smallest component of the five P classes taking up only $6 \pm 8\%$ of TPP, which was similar to 6–15% of Amazon River (Berner and Rao, 1994) and 4.6% of Florida Bay (Zhang et al., 2004).

Refractory organic P, generally higher during the spring and the summer but lower during the fall and the winter (Fig. 3A), was on average $29 \pm 11\%$ of TPP at 500 m but $36 \pm 11\%$ of TPP at 1500 m of the XS station. This values were comparable to 24% of the Florida Bay sediments but higher than 10% of the Arctic sediments (Zhang et al., 2010). Higher percentage of refractory organic P found at the XS station would reflect its higher primary productivity compared to other regions (Ma et al., 2011).

3.2. Variability of sinking particulate phosphorus including TPP, POP, and PIP

TPP of sinking particles at the 500 m XS sediment trap varied substantially from 10.1 to 115.1 µmol P g^{-1}. An averaged TPP of 47.0 ± 26.3 µmol P g^{-1} in the upper traps was similar to the suspended particles in the Gulf of California (Lyons et al., 2011), but was higher than that in the Yukon River (Guo et al., 2004). Except for September 2012, TPP was generally much higher ($t=4.92$, $p < 0.01$, df=32) in the upper trap (50.5 ± 25.4 µmol P g^{-1}) than in the lower trap (23.1 ± 11.6 µmol P g^{-1}) (Fig. 4A).

Unlike along the southern California coast where ~85% of the TPP was PIP (Sekula-Wood et al., 2012), sinking POP dominated the total particulate phosphorus in the western NSCS, accounting for $52 \pm 11\%$ and $55 \pm 9\%$ of TPP at 500 m and 1500 m (Fig. 3), respectively. POP in the upper traps was generally higher ($t=4.71$, $p < 0.01$, df=18) in the spring-summer than in the fall-winter during our study period, largely due to seasonal change of refractory organic P (Fig. 3A). Higher refractory organic P in the spring-summer may likely be caused by higher riverine inputs during these wet seasons.

There was large difference in PIP composition of sinking particle between the two layers at XS. Fe-bound inorganic P dominated the PIP pool at 500 m ($53 \pm 14\%$), following by CaCO$_3$-bound inorganic P ($18 \pm 11\%$), adsorbed inorganic P ($18 \pm 8\%$), and detrital P ($11 \pm 12\%$) (Fig. 3C), while detrital P ($46 \pm 12\%$) and CaCO$_3$-bound inorganic P ($30 \pm 8\%$) were two the most important PIP components at 1500 m with negligible adsorbed and Fe-bound inorganic P (Fig. 3D). There was, however, no clear seasonal variability of PIP during the two years of sampling.

3.3. Time-series variation of sinking fluxes of total mass, particulate phosphorus and biogenic silica

During our sampling period, total mass flux of sinking particles at the 500 m XS station was in a range of 20.7–208.3 mg m^{-2} d^{-1} (on average 78 ± 50 mg m^{-2} d^{-1}), which was comparable with ~100 mg m^{-2} d^{-1} at 1000 m of the central NSCS (Lahajnar et al., 2007). There was generally higher total mass flux ($t=6.51$, $p < 0.01$, df=11) at 500 m in the winter (99.9 ± 32.8 mg m^{-2} d^{-1}) than in the summer (41.6 ± 15.4 mg m^{-2} d^{-1}) (Fig. 4C). TMF in the lower traps varied more broadly from 38.2 to 842.2 mg m^{-2} d^{-1}. The averaged TMF of 281 ± 229 mg m^{-2} d^{-1} at 1500 m was about four times of that at 500 m (Fig. 4C). Previous observations at the 1500 m XS station had documented several peaks of TMF occurring in November 2010, December 2011, March 2012, and August 2012, respectively (Liu et al., 2014). We continued to observe substantially higher TMF at 1500 m in October 2012, February 2013, June 2013, and October 2013 (Fig. 5).

Both sinking particulate P and opal fluxes at the 1500 m XS station showed similar high values in October 2012, February 2013, June
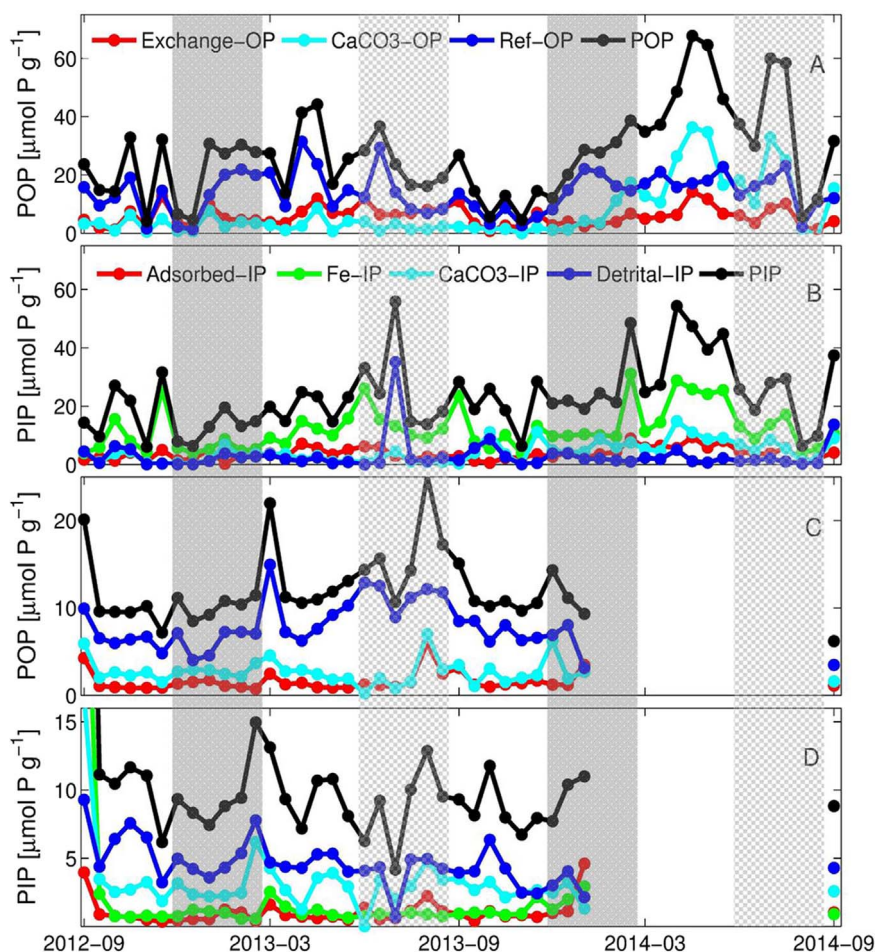
Fig. 3. Temporal variations of particulate organic phosporus (POP), including exchangeable organic P, CaCO₃-bound organic P, and refractory organic P, and particulate inorganic phosphorus (PIP), including adsorbed inorganic P, Fe-bound inorganic P, CaCO₃-bound inorganic P, and detrital apatite P, of sinking particles in the upper (A, B) and lower traps (C, D) of the Xisha station. The shaded areas represent winter (gray) and summer (light gray) and the white areas are spring and autumn of each year.

2013, and October 2013 (Fig. 4D and E). In contrast to those observed in the upper trap (50.5 ± 25.4 μmol P g^{-1} and 0.8 ± 0.7 mmol Si g^{-1}), settling particles at the lower trap contained much less particulate P (23.1 ± 11.6 μmol P g^{-1}, $t=-5.74$, $p < 0.01$, df=32) but more opal (1.3 ± 0.7 mmol Si g^{-1}, $t=2.97$, $p < 0.01$, df=31). Consequently, the ratio of opal to POP was much higher in the lower trap near the ocean floor. Our data also revealed substantially higher opal fluxes (0.20 ± 0.09 mmol Si m^{-2} d^{-1}, $t=4.93$, $p < 0.01$, df=5) during the winter of 2013 at the 500 m XS station (Fig. 4E), in addition to an increased opal content of sinking particles (Fig. 4B). The enhanced sinking opal content and export flux during this period of time in the upper trap could result from diatom intrinsic organic matter (Robinson et al., 2004) due to enhanced primary productivity (Fig. 5).

3.4. Mechanisms for temporal change in sinking particulate phosphorus concentration, composition, and fluxes in the upper ocean

In the coastal ocean, temporal variations of total mass fluxes and particulate phosphorus fluxes of sinking particles would be generally controlled by riverine discharge (Sekula-Wood et al., 2012). Particle flux at XS however was less influenced by riverine inputs since the station is remote from the major rivers discharging into the NSCS. There was a general seasonal cycle of depth-integrated primary productivity (IPP) at XS with higher productivity in the winter but lower productivity in the summer (Fig. 5). Except for the summer of 2012, the temporal variation of TMF at 500 m generally followed that of IPP within the euphotic zone from June 2009 to September 2014. High particle flux in the summer of 2012 might be related to lateral

eddy transport of riverine turbidity, which could lead to enhanced particle export in the upper ocean by submesoscale dynamics (Zhou et al., 2013). The significant correlation between TMF and IPP ($r^2=0.4$, $p < 0.05$, df=85) would suggest a rapid transport of particles to the seafloor. This result indicated that primary production might play an important role on sinking particle flux at XS of the NSCS. The finding is consistent with reports of high POC export near Xisha compared to other regions (Ma et al., 2011), though concurrent POC/PON measurements are not available. The majority of sinking P at XS was composed of marine biologically produced POP, which was quite different from those in the coastal setting where PIP dominated TPP (Faul et al., 2005; Lyons et al., 2011). Besides physical process affecting particle settling in the water column, fluxes of biogenic particulate organic materials sinking to the deep ocean should be largely controlled by primary production in the euphotic zone above (Lahajnar et al., 2007).

Interestingly, there were increased total particulate phosphorus contents of sinking particles at 500 m during 2014 (Fig. 4A), as well as substantially higher concentrations of CaCO₃-bound P and higher percentages of CaCO₃-bound P in TPP (Figs. 3 and 6). The increased CaCO₃-bound P and TPP were largely contributed by CaCO₃-bound organic P (Fig. 3A). Due to its high carrying capacity for POP, carbonate minerals played an important role in transporting POP to the deep ocean (Sekula-Wood et al., 2012), which was different from the ordinary case of sinking POC controlled by particle aggregation (Passow, 2002; Sun et al., 2012). The increased role of CaCO₃-bound P on sinking particulate phosphorus during 2014 might indicate an enhanced carbonate deposition at the XS station, since the ratio of POP to CaCO₃ is generally constant in the upper ocean. One of the most
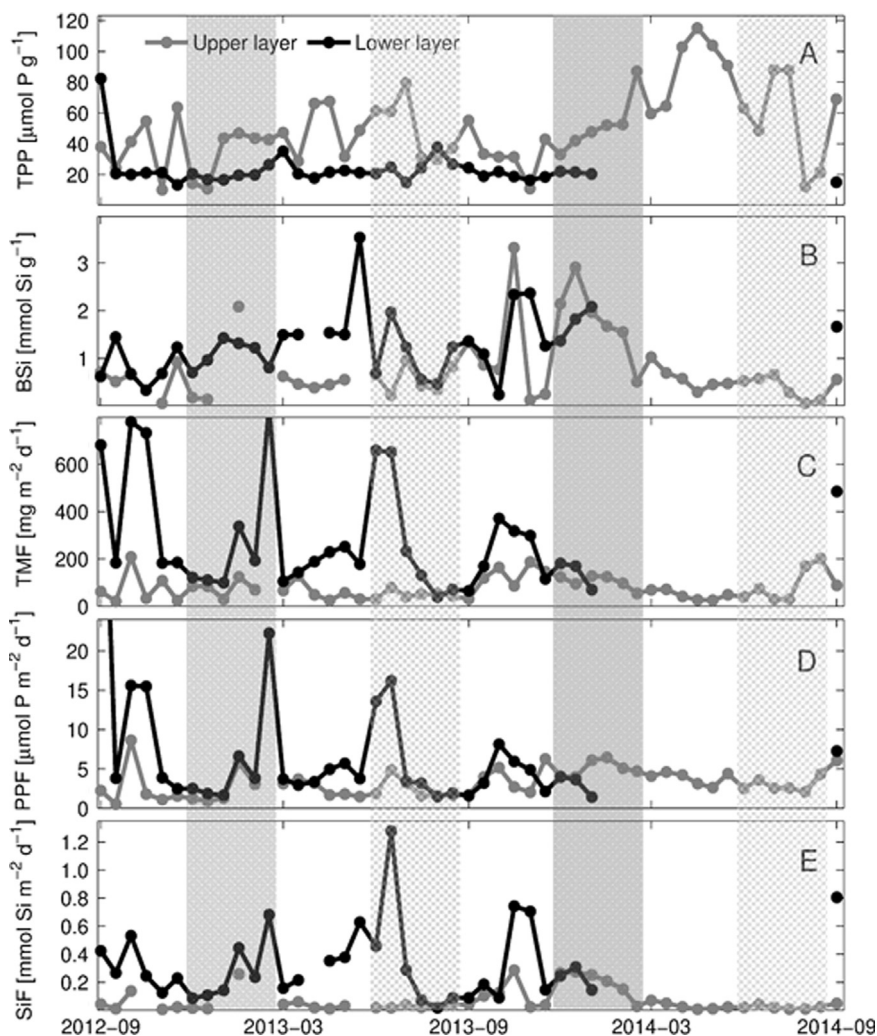
Fig. 4. Temporal variations of (A) total particulate phosphorus (TPP), (B) biogenic silica (BSi), (C) total mass flux (TMF), (D) particulate phosphorus flux (PPF), and (D) biogenic silica flux (SiF) in the upper and lower traps of the XS station. The shaded areas represent winter (gray) and summer (light gray) and the white areas are spring and autumn of each year.
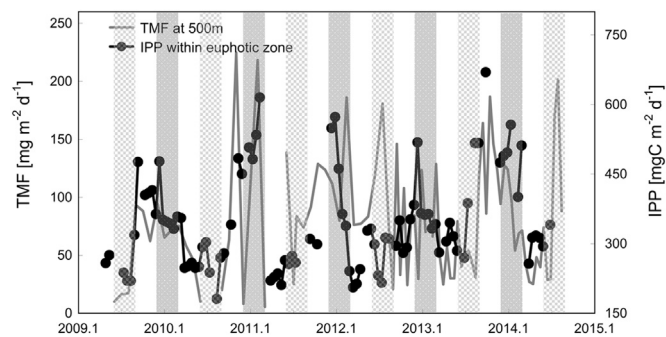

Fig. 5. Comparisons of total mass flux (TMF) at 500 m and the depth-integrated primary production (IPP) at the XS station from 2009 to 2015. IPP are derived data from NOAA's monthly Aqua MODIS and Pathfinder products. TMF data from 2009 to 2012 is reproduced from Liu et al. (2014) The shaded areas represent winter (gray) and summer (light gray) and the white areas are spring and autumn of each year.
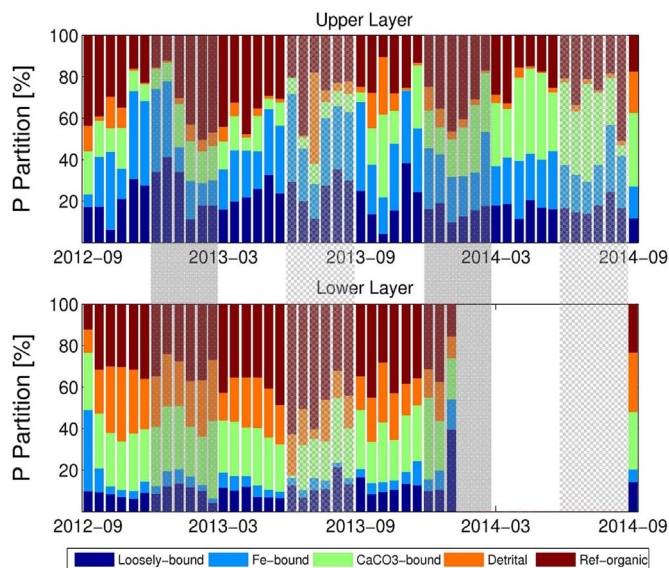

Fig. 6. Temporal variations of sinking particulate phosphorus composition in the upper and lower traps of the XS station. The shaded areas represent winter (gray) and summer (light gray) and the white areas are spring and autumn of each year.
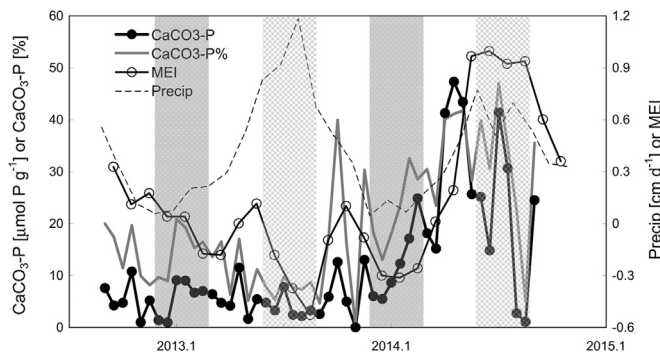
possible causes for change of carbonate deposition at XS would be the El Niño /Southern Oscillation (ENSO). In fact, the period of increased CaCO$_3$-bound P and TPP at Xisha during 2014 was accompanied by a strong El Niño event (Fig. 7). The effect of El Niño on ocean circulation

Fig. 7. Comparisons of the concentration of $CaCO_3$-bound P and the percentage of $CaCO_3$-bound P in TPP of the sinking particles at the upper trap of the Xisha station with the multivariate ENSO index (MEI) and the precipitation rate (Precip). The shaded areas represent winter (gray) and summer (light gray) and the white areas are spring and autumn of each year.

would be expected to increase the stratification thus decrease the upwelling of CO_2-rich deep water (Jones et al., 2001), leading to increased pH and over-saturation of seawater with respect to calcite at the surface layer, a condition in favor of abiotic precipitation of $CaCO_3$ and subsequent sinking of newly formed $CaCO_3$ to the ocean interior. On the other hand, temperature increased with El Niño might lead to an ecological shift from diatom toward calcifiers (Sett et al., 2014), which would also contribute to $CaCO_3$ deposition at XS. In fact, carbon export by $CaCO_3$ deposition is relatively abundant in the Xisha region compared to the central NSCS (Cao et al., 2009). The El Niño related increase of $CaCO_3$-bound P during 2014, however, was accompanied by relatively lower opal, POP, and total mass fluxes. The lower particle fluxes under strong El Niño at Xisha may likely be driven by reduced rainfall compared to the summer of 2013 (Fig. 7). Reductions of opal and organic carbon fluxes but increase of $CaCO_3$ content of sinking particle in the western subtropical Pacific had been attributed to suppression of biological productivity by reduced rainfall as a result of shift of the western Pacific warm pool during the strong El Niño of 2009/2010 (Kim et al., 2014).

3.5. What controls the variability of sinking particles fluxes in the deep ocean near the seafloor?

Based on clay mineral composition of trap samples at XS, the settling particles of the Xisha may contain particles from Taiwan transported by ocean currents (Liu et al., 2014). However, it is difficult to explain the large peaks of particle flux measured with the traps deployed closed to the seafloor by lateral transport over such long distance considering the relatively constant velocity of 5−6 cm s^{-1} and direction of 170°−180° of bottom currents (Liu et al., 2014). Earthquakes could generate turbidity flows near the bottom of the Xisha Trough (Qin et al., 2015) and supply laterally transported material. There were indeed some correlations between the peaks of TMF of the deeper traps and the peaks of earthquake intensities (magnitudes and depths) recorded in the nearby Hainan Island from September 2012 to August 2013 (Figs. 4C and 8). However, we could not explain the inverse relationship between TMF and earthquake intensity during the fall and winter of 2013.

Our results suggested that the abnormal high TMF at the lower traps is a result of sediment resuspension (Fig. 4C). Firstly, the resuspension argument is supported by the similarity of P contents between the settling particles and the seafloor sediments. The mean TPP of ~21 μmol P g^{-1} in sinking particles of the lower traps are about the same as 22.73 μmol P g^{-1} of the surface sediments at XS (Dang et al., 2013), suggesting the sediment source of particles to the lower traps. Secondly, higher percentage of detrital P (46%) at the lower traps would support the terrestrial source of sinking particles by resuspension. Thirdly, we observed high percentage
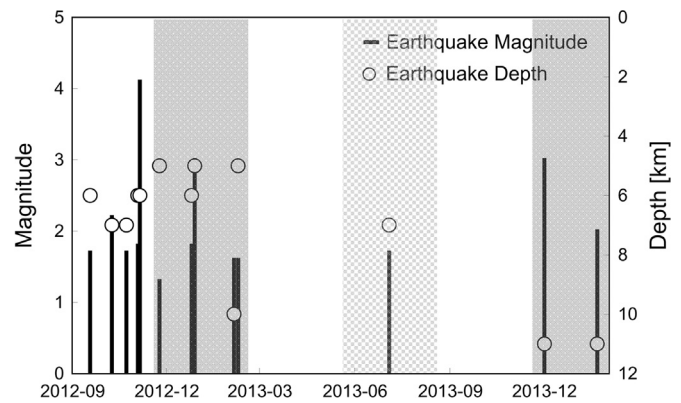

Fig. 8. Magnitudes and depths of the recorded earthquakes in the southeast Hainan Island from September 2012 to February 2014. Data are taken from the China Earthquake Data Center (http://data.earthquake.cn/data/index.jsp). The shaded areas represent winter (gray) and summer (light gray) and the white areas are spring and autumn of each year.

(~58%) of organic P in the $CaCO_3$-bound P in the near-bottom traps, which again would support the importance of benthic input by carbonate sediments, similar to the case in Florida Bay (Zhang et al., 2004). Finally, higher opal to POP ratios of sinking particles in the lower traps could be a result of sediment resuspension, as marine sediments are rich in biogenic silica due to the high efficiency of opal preservation than organic matter during particle depositions (Nelson et al., 1996).

Sediment resuspension in the deep ocean could be driven by variations in near-bottom shear stresses (Lesht, 1979). It had been suggested that resuspension of rebound particles, settled through the water column before being incorporated into the sediments, may account for the high particle fluxes observed near the ocean floor (Walsh et al., 1988). To investigate the relationship between the resuspended particles collected in our sediment traps and the suspended particles in the water column, we applied a two-component mixing model (Bonnin et al., 2002) with the assumption that TMF includes a constant background flux (S_0) with a P content of C_0 and a variable rebound flux S_r with a P content of C_r from resuspension: $TMF \times POP = S_0 \times C_0 + S_r \times C_r$. Substituting S_r by $TMF - S_0$, we can get the POP content of the flux as

$$POP = (C_0 - C_r) \times \frac{S_0}{TMF} + C_r$$

The box model is rather simple by assuming a constant primary flux of sinking particles, which is approximately satisfied by the fact that the background TMF of the lower traps was relatively constant (131 ± 48 mg m^{-2} d^{-1}) and was comparable to TMF of the upper traps (97 ± 47 mg m^{-2} d^{-1}) that was not affected by sediment resuspension. These fluxes are orders of magnitude lower than those in the North Sea (Walsh et al., 1988; Bonnin et al., 2002). By the regression of POP against TMF using the above equation for the entire sediment trap dataset (Fig. 9), we can estimate C_r of 2.3%, which is well consistent with those of 2.3−4.2% for POP reported in the surface sediments of the NSCS (Wang et al., 2013; Dang et al., 2013).

3.6. P cycle inferred from difference of particulate P composition

Since large quantities of riverine particles are caught-up within estuaries, input of DIP from rivers is recognized as the major source of P to the ocean (Paytan and McLaughlin, 2007). Particulate P could be produced through DIP adsorption of suspended particles (Ruttenberg and Berner, 1993) or by resuspension of P-rich sediment in the coastal ocean, in addition to POP production by marine phytoplankton. These particulate P would be recycled in the water column with only a small fraction escaping from the rapid regeneration and being delivered to
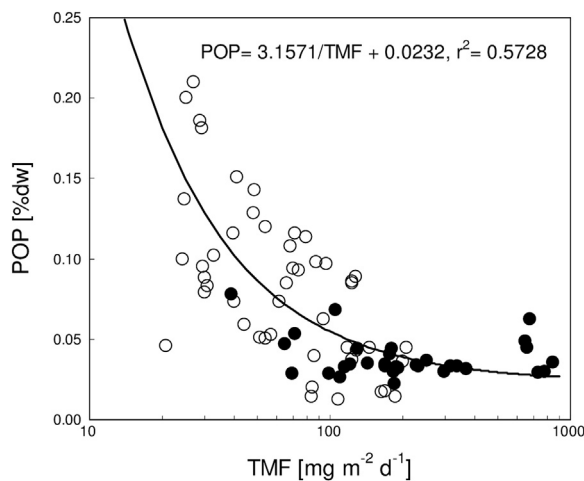
Fig. 9. Relationship between total mass flux (TMF) and POP content of sinking particles at XS. Open circles are data of the upper traps with black dots for the lower traps; the regression line shows the fitting of two-component model (see text for detail).
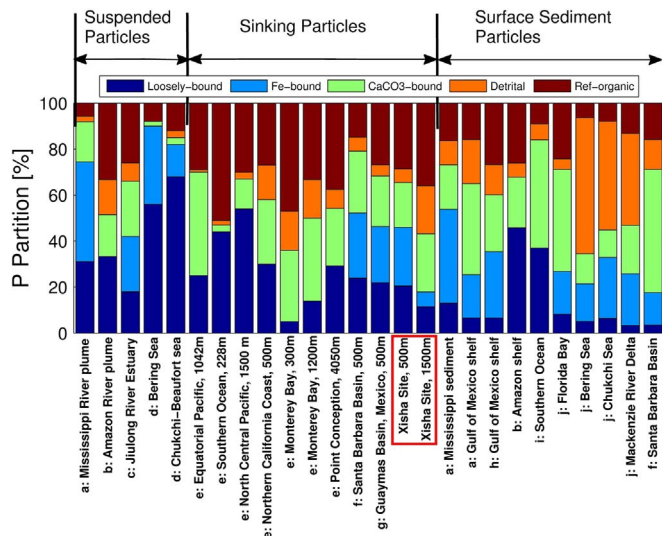

Fig. 10. Particulate P composition in various coastal and oceanic particulate matter including suspended particles at sea surface, sinking particles, and surface sediment particles. The red rectangle shows the mean values at XS. Data include (a) Sutula et al. (2004), (b) Berner and Rao (1994), (c) Lin et al. (2013), (d) Lin et al. (2012), (e) Faul et al. (2005), (f) Sekula-Wood et al. (2012), (g) Lyons et al. (2011), (h) Ruttenberg and Berner (1993), (i) Latimer et al. (2006), and (j) Zhang et al. (2004, 2010). Note that only four P classes are reported in b, e, and I, in which loosely-bound and Fe-bound P were combined into one fraction.

the seafloor (Benitez-Nelson, 2007). The sinking particulate P reaching the seafloor would be eventually buried together with organic material and metal oxyhydroxides in sediments (Delaney, 1998). Because labile inorganic and organic P species in the particles will be preferentially remineralized and lost to seawater during particle setting and burying processes, one would expect to observe a significant difference in P composition among suspended particles nearshore, sinking particles in the open seas, and sediment particles on the seafloor.

Fig. 10 showed the particulate P composition from various particles collected in the coastal and oceanic environments, including suspended particles at sea surface (collected by filtration), sinking particles (collected by sediment traps deployed at depth), and surface sediment particles (by coring or grapping). Based on compiled data from different marine environments, we found significantly lower percentage of labile P including loosely-bound P and Fe-bound P ($t=-2.99$, $p <$ 0.01, df=4) of sinking particles ($33 \pm 16\%$) compared to that of suspended particles ($64 \pm 25\%$). This difference could result from

conversion of labile P to $CaCO_3$-bound P and refractory organic P during the particle sinking process (Sutula et al., 2004). Indeed, we found substantially higher ($t > 2.76$, $p < 0.01$, df=4) refractory organic P of sinking particles ($33 \pm 10\%$) than suspended particles ($17 \pm 11\%$) and sediment particles ($16 \pm 7\%$). High refractory organic P composition in sinking particles should reflect high biological production in the surface ocean. Interestingly, we found significantly higher ($t=2.23$, $p <$ 0.01, df=4) $CaCO_3$-bound P in the TPP of the surface sediment particles ($30 \pm 15\%$) than those of sinking particles and suspended particles ($13 \pm 10\%$). Due to microbial utilization and reduction of organic matter, the organic P of marine sediments could also be readily transformed into $CaCO_3$-bound inorganic P phases, specifically authigenic carbonate fluorapatite, through processes such as sink-switching (Ruttenberg and Berner, 1993). In contrast, authigenic carbonate fluorapatite is less important for $CaCO_3$-bound P in sinking particles (Sekula-Wood et al., 2012). These results support previous findings that $CaCO_3$-bound P is the major sedimentary sink of P in the global P cycle (Rutternberg and Berner, 1993; Paytan and McLaughlin, 2007). In summary, difference in particulate P composition of the suspended particles, sinking particles, and sediment particles may be tightly related to the biogeochemical cycling of P in the ocean.

4. Conclusions

In this paper, we present the first detailed study of phosphorus forms of sinking particles in the NSCS. Our time-series observations revealed substantial variations of sinking particulate phosphorus concentrations and composition during the two year study period. Seasonal change of POP that dominated the TPP in the NSCS was largely contributed by refractory organic P. Large change of PIP composition was found at depths with Fe-bound inorganic P and $CaCO_3$-bound inorganic P dominated the PIP pool in the upper trap, but detrital P and Fe-bound inorganic P in the lower trap. We also found much higher ratios of opal to POP near the seafloor than in the upper ocean suggesting the important role of sediment inputs.

From June 2009 to September 2014, temporal change of sinking particle flux in the upper trap was found largely controlled by primary production of the NSCS. Enhanced surface productivity had resulted in higher TPP and POP fluxes as well as higher opal flux in the upper ocean. Higher concentration of TPP and the percentage of $CaCO_3$-bound P in TPP in the upper ocean during the year of 2014 were largely contributed by $CaCO_3$-bound organic P, which may be induced by ENSO related change of calcium carbonate deposition at Xisha. The intense peaks of particle flux near the seafloor of Xisha could be largely attributed to sediment resuspension at Xisha. By applying a two-component mixing model of resuspension processes to our data, we predicted a POP content of 2.32% for the resuspended sediments at XS that agreed well with previous results in the NSCS.

References

Behrenfeld, M.J., Falkowski, P.G., 1997. Photosynthetic rates derived from satellite-based chlorophyll concentration. Limnol. Oceanogr. 42 (1), 1–20.

Benitez-Nelson, C.R., Buesseler, K.O., 1999. Variability of inorganic and organic phosphorus turnover rates in the coastal ocean. Nature 398, 502–505.

Benitez-Nelson, C.R., Madden, L.P.O., Styles, R.M., Thunell, R.C., Astor, Y., 2007. Inorganic and organic sinking particulate phosphorus fluxes across the oxic/anoxic water column of Cariaco Basin, Venezuela. Mar. Chem. 105, 90–100.

Berner, R.A., Rao, J.L., 1994. Phosphorus in sediments of the Amazon River and estuary: implications for the global flux of phosphorusp to the sea. Geochim. Cosmochim. Acta 58, 2333–2339.

Bjorkman, K., Karl, D.M., 2003. Bioavailability of dissolved organic phosphorus in the euphotic zone at Station ALOHA, North Pacific Subtropical Gyre. Limnol. Oceanogr. 48, 1049–1057.

Bonnin, J., van Raapporst, W., Brummer, G., van Haren, H., Malschaert, H., 2002. Intense mid-slope resuspension of particulate matter in the Faeroe-Sheland Channel: short-term deployment of near-bottom sediment traps. Deep-Sea Res. Part I 49, 1485–1505.

Cao, Z., Dai, M., Lu, Z., Zhou, K., 2009. $CaCO_3$ to organic carbon ratio in the South China Sea. Adv. Geosci. 12, 109–125.

Chen, W., Cai, P., Dai, M., Wei, J., 2008. $^{234}Th/^{238}U$ disequilibrium and particulate organic carbon export in the northern South China Sea. J. Oceanogr. 64, 417–428.

Dang, H., Yang, J., Li, J., Luan, X., Zhang, Y., Gu, G., Xue, R., Zong, M., Klotz, M.G., 2013. Environment-dependent distribution of the sediment *nif*H-harboring microbiota in the northern South China Sea. Appl. Environ. Microbiol. 79 (1), 121–132.

Delaney, M.L., 1998. Phosphorus accumulation in marine sediments and the oceanic phosphorus cycle. Global Biogeochem. Cycles 12, 563–572.

Diaz, J., Ingall, E., Benitez-Nelson, C., Paterson, D., de Jonge, M.D., McNulty, lan, Brandes, J.A., 2008. Marine polyphosphate: A key player in geologic phosphorus sequestration. Science 320 (5876), 652–655.

Faul, K.L., Paytan, A., Delaney, M.L., 2005. Phosphorus distribution in sinking oceanic particulate matter. Mar. Chem. 97, 307–333.

Francois, R., Honjo, S., Bacon, M.P., 2001. Deep-Sea Moored Sediment traps: How accurate are they at recording the vertical flux of settling particles? Oceanography 14, 65–66.

Guo, L., Semiletov, I., Gustafsson, O., Ingri, J., Andersson, P., Dudarev, O., White, D., 2004. Characterization of Siberian Arctic estuarine sediments: implications for terrestrial organic carbon export. Global Biogeochem. Cycles 18 (1), GB1036. http://dx.doi.org/10.1029/2003GB002087.

Huang, X.L., Zhang, J.-Z., 2009. Neutral persulfate digestion at sub-boiling temperature in an oven for total dissolved phosphorus determination in natural waters. Talanta 78, 1129–1135.

Ho, T., You, C., Chou, W., Pai, S., Wen, L., Sheu, D.D., 2009. Cadmium and phosphorus cycling in the water column of the South China Sea: The roles of biotic and abiotic particles. Mar. Chem. 115, 125–133.

Honjo, S., Manganini, S.J., Krishfield, R.A., Francois, R., 2008. Particulate organic carbon fluxes to the ocean interior and factors controlling the biological pump: A synthesis of global sediment trap programs since 1983. Prog. Oceanogr. 76, 217–285.

Jones, C.D., Collins, M., Cox, P.M., Spall, S.A., 2001. The carbon cycle response to ENSO: a coupled climate-carbon cycle model study. J. Climate 14 (21), 4113–4129.

Kim, H., Hyeong, K., Park, J., Jeong, J., Jeon, D., Kim, E., Kim, D., 2014. Influence of Asian monsoon and ENSO events on particle fluxes in the western subtropical Pacific. Deep-Sea Res. Part I 90, 139–151.

Latimer, J.C., Filippelli, G.M., Hendy, I., Newkirk, D.R., 2006. Opal-associated particulate phosphorus: Implications for the marine P cycle. Geochimica et Cosmochimica Acta 70, 3843–3854.

Lahajnar, N., Wiesner, M.G., Gaye, B., 2007. Fluxes of amino acids and hexosamines to the deep South China Sea. Deep-Sea Res. Part I 54, 2120–2144.

Lesht, B.M., 1979. Relationship between sediment resuspension and the statistical frequency distribution of bottom shear stress. Mar. Geol. 32 (1-2), M19–M27.

Li, Q.P., Hansell, D.A., 2008. Intercomparison and coupling of magnesium induced coprecipitation and long-path liquid waveguide capillary cell techniques for trace analysis of phosphate in seawater. Anal. Chim. Acta 611, 68–72.

Li, Q.P., Hansell, D.A., Zhang, J.Z., 2008. Underway monitoring of nanomolar nitrate plus nitrite and phosphate in oligotrophic seawater. Limnol. Oceanogr. Methods 6, 319–326.

Li, Q.P., Wang, Y., Dong, Y., Gan, J., 2015. Modeling of long-term variability of planktonic ecosystems in the northern South China Sea and the upstream Kuroshio. J. Geophys. Res. 120. http://dx.doi.org/10.1002/2014JC010609.

Liebezeit, G., 1991. Analytical phosphorus fractionation of sediment trap material. Mar. Chem. 33, 61–69.

Lin, P., Guo, L., Chen, M., Cai, Y., 2013. Distribution, partitioning and mixing behavior of phosphorus species in the Jiulong River EstuaryE. Mar. Chem. 157, 93–105.

Lin, P., Guo, L., Chen, M., Tong, J., Lin, F., 2012. The distribution and chemical speciation of dissolved and particulate phosphorus in the Bering Sea and the Chukchi-Beaufort Seas. Deep-Sea Res. Part II 81-84, 79–94.

Liu, J., Clift, P.D., Yan, W., Chen, Z., Chen, H., Xiang, R., Wang, D., 2014. Modern transport and deposition of settling particles in the northern South China Sea: Sediment trap evidence adjacent to Xisha Trough. Deep-Sea Res. Part I 93, 145–155.

Liu, K., Chao, S., Shaw, P., Gong, G., Chen, C., Tang, T., 2002. Monsoon-forced chlorophyll distribution and primary production in the South China Sea:

observations and a numerical study. Deep-Sea Res. Part I 49, 1387–1412.

Lyons, G., Benitez-Nelson, C., Thunell, R., 2011. Phosphorus composition of sinking particles in the Guaymas Basin, Gulf of California. Limnol. Oceanogr. 56, 1093–1105.

Ma, H., Zeng, Z., Yu, W., He, J., Chen, L., Cheng, J., Yin, M., Zeng, S., 2011. $^{234}Th/^{238}U$ disequilibrium and particulate organic carbon export in the northwestern South China Sea. Acta Oceanol. Sinica 30 (3), 55–62.

Millero, F., Huang, F., Zhu, X., Liu, X., Zhang, J.Z., 2001. Adsorption and desorption of phosphate on calcite and aragonite in seawater. Aquatic Geochemistry 7 (1), 33–56.

Mortlock, R.A., Froelich, P.N., 1989. A simple method for the rapid determination of biogenic opal in pelagic marine sediments. Deep-Sea Res. 36, 1415–1426.

Nelson, D.M., DeMaster, D.J., Dunbar, R.B., Smith, W.O., Jr., 1996. Cycling of organic carbon and biogenic silica in the Southern Ocean: estimates of water-column and sedimentary fluxes on the Ross Sea continental shelf. J. Geophys. Res. 101, 18519–18532.

Paytan, A., McLaughlin, K., 2007. The oceanic phosphorus cycle. Chemical Review 107, 563–576.

Passow, U., 2002. Transparent exopolymer particles (TEP) in aquatic environments. Prog. Oceanogr. 55, 287–333.

Qin, Z., Wu, S., Wang, D., Li, W., Gong, S., Mi, L., Geroge, S., 2015. Mass transport deposits and processes in the north slope of the Xisha Trough, northern South China Sea. Acta Oceanol. Sin. 34, 117–125.

Robinson, R.S., Brunelle, B.G., Sigman, D.M., 2004. Revisiting nutrient utilization in the glacial Antarctic: evidence from a new method for diatom-bound N isotopic analysis. Paleoceanogr 19, PA3001. http://dx.doi.org/10.1029/2003PA000996.

Ruttenberg, K.C., 1992. Development of a sequential extraction method for different forms of phosphorus in marine sediments. Limnol. Oceanogr. 37, 1460–1482.

Ruttenberg, K.C., Berner, R.A., 1993. Authigenic apatite formation and burial in sediments from non-upwelling, continental margin environments. Geochim. Cosmochim. Acta 57, 991–1007.

Sekula-Wood, E., Benitez-Nelson, C.R., Bennett, M.A., Thunell, R., 2012. Magnitude and composition of sinking particulate phosphorus fluxes in Santa Barbara Basin, California. Global Biogeochem. Cycles 26, GB2023. http://dx.doi.org/10.1029/2011GB004180.

Sett, S., Bach, L.T., Schulz, K.G., Koch-Klavsen, S., Lebrato, M., Riebesell, U., 2014. Temperature modulates Coccolithophorid sensitivity of growth, photosynthesis and calcification to increasing seawater pCO2. PloS ONE 9 (2), 688308. http://dx.doi.org/10.1371/journal.pone.0088308.

Sun, C., Wang, Y., Li, Q.P., et al., 2012. Distributional characteristics of transport exopolymer particles in the Pearl River Estuary, China. J. Geophys. Res. 117. http://dx.doi.org/10.1029/2012jg001951.

Sutula, M., Bianchi, T.S., McKee, B.A., 2004. Effect of seasonal sediment storage in the lower Mississippi River on the flux of reactive particulate phosphorus to the Gulf of Mexico. Limnol. Oceanogr. 49 (6), 2223–2235.

Tyrrell, T., 1999. The relative influence of nitrogen and phosphorus on oceanic primary production. Nature 400, 525–531.

Wang, L., Ye, M., Li, Q., Zou, H., 2013. Phosphorus speciation in wetland sediments of Zhujiang (Pearl) River Estuary, China. Chin. Geograph. Sci. 23, 574–583.

Walsh, I., Fischer, K., Murray, D., Dymond, J., 1988. Evidence for resuspension of rebound particles from near-bottom sediment traps. Deep-Sea Res. 35 (1), 59–70.

Wei, C., Lin, S., Sheu, D.D., Chou, W., Yi, M., Santschi, P., Wen, L., 2011. Particle-reactive radionuclides (^{234}Th, ^{210}Pb, ^{210}Po) as tracers for the estimation of export production in the South China Sea. Biogeosciences 8, 3793–3808.

Wu, J.F., Chung, S.W., Wen, L.S., Liu, K.K., Chen, Y.L.L., Chen, H.Y., Karl, D.M., 2003. Dissolved inorganic phosphorus, dissolved iron, and Trichodesmium in the oligotrophic South China Sea. Global Biogeochem. Cycles 17 (1), 1008. http://dx.doi.org/10.1029/2002GB001924.

Xu, J., Yin, K., He, L., Yuan, X., Ho, A.Y.T., Harrison, P.J., 2008. Phosphorus limitation in the northern South China Sea during late summer: Influence of the Pearl River. Deep-Sea Res. Part I 55 (10), 1330–1342.

Yin, K., Song, X., Sun, J., Wu, M., 2004. Potential P limitation leads to excess N in the Pearl River estuarine coastal plume. Cont. Shelf Res. 24 (16), 1895–1907.

Yoshimura, T., Nishioka, J., Saito, H., Takeda, S., Tsuda, A., Wells, M.L., 2007. Distributions of particulate and dissolved organic and inorganic phosphorus in North Pacific surface waters. Mar. Chem. 103, 112–121.

Zhang, J.-Z., Fischer, C.J., Ortner, P.B., 2004. Potential availability of sedimentary phosphorus to sediment resuspension in Florida Bay. Global Biogeochem. Cycles 18, GB4008.

Zhang, J.-Z., Guo, L., Fischer, C., 2010. Abundance and chemical speciation of phosphorus in sediments of the Mackenzie River Delta, the Chukchi Sea and the Bering Sea: Importance of detrital apatite. Aqua. Geochem. 16, 353–371.

Zhou, K., Dai, M., Kao, S., Wang, L., Xiu, P., Chai, F., Tian, J., Liu, Y., 2013. Apparent enhancement of ^{234}Th-based particle export associated with anticyclonic eddies. Earth Planet. Sci. Lett. 381, 198–209.